Development of a battery real-time state of health diagnosis based on fast impedance measurements

This document is the pre-print version of the article:
Locorotondo, E., Cultrera, V., Pugi, L., Berzi, L., Pierini, M., Lutzemberger, G., 2021. Development of a battery real-time state of health diagnosis based on fast impedance measurements. Journal of Energy Storage 38, 102566.
https://doi.org/10.1016/j.est.2021.102566

Development of a battery real-time state of health diagnosis based on fast impedance measurements

Edoardo Locorotondo[a], Vincenzo Cultrera[a], Luca Pugi[a], Lorenzo Berzi[a], Marco Pierini[a] Giovanni Lutzemberger[b],

[a]DIEF (Industrial Engineering Department)
University of Florence Firenze- Italy

[b]DESTEC (Department of Energy, Systems, Territory and Constructions Engineering)
University of Pisa Pisa- Italy

ABSTRACT

The capability to assess and monitor the state of health (SOH) of lithium-based cells is a highly demanded feature for advanced battery management systems. Due to the existing relation between SOH and internal impedance, electrochemical impedance spectroscopy (EIS) methods are adopted for SOH diagnosis. Nevertheless, accurate EIS tests demand expensive facilities, long time test procedures, and algorithms with high-computational efforts, which makes them almost unsuitable for on-board systems. This paper presents a new diagnostic method aimed at detecting battery SOH using fast impedance measurements. Key factor is the application of a broadband current signal excitation on the battery; for the application here presented, a pseudo-random binary sequence (PRBS) excitation is adopted. To demonstrate the functionalities of a prototype testbed, several cells of the same manufacturer but presenting different SOHs, due to their past load history, have been subjected to the EIS test, acquiring voltage response under imposed excitation. Finally, test results have been processed: the key step being the clustering of impedance measurements (represented in Nyquist diagram) in different rectangular areas, which are related to actual SOH. The performed experimental test results showed the possibility to determine frequency points in which the impedance measurements dramatically change due to different cell SOH; as a consequence, these peculiar frequencies can be adopted as reference for cluster separation. According to the results here presented, the proposed method is sufficiently accurate and is a promising solution for real-time diagnostic of battery health thanks to its simplicity and speed.

Keywords: Lithium-ion battery; second life; end of life; state of health; electrochemical impedance spectroscopy; PRBS; ordinary coherence; electric vehicle.

This document is the pre-print version of the article:
Locorotondo, E., Cultrera, V., Pugi, L., Berzi, L., Pierini, M., Lutzemberger, G., 2021. Development of a battery real-time state of health diagnosis based on fast impedance measurements. Journal of Energy Storage 38, 102566.
https://doi.org/10.1016/j.est.2021.102566

NOMENCLATURE

EIS	Electrochemical impedance spectroscopy
LIB	Lithium battery
EV	Electric vehicle
HEV	Hybrid electric vehicle
ICE	Internal combustion engine
EOL	End of life
SOL	State of life
SOH	State of health
SOC	State of charge
C	Battery nominal capacity (in Ah)
$z[n]$	Impulse response
$Z(k)$	Frequency response
k	Normalized frequency
N	Total harmonics number
R_0	Series resistance used in sample impedance circuit
R_1	RC resistance used in sample impedance circuit
C_1	RC capacitance used in sample impedance circuit
R_p	Parasitic resistance in capacitance C_1
R_{int}	Internal resistance

This document is the pre-print version of the article:
Locorotondo, E., Cultrera, V., Pugi, L., Berzi, L., Pierini, M., Lutzemberger, G., 2021. Development of a battery real-time state of health diagnosis based on fast impedance measurements. Journal of Energy Storage 38, 102566.
https://doi.org/10.1016/j.est.2021.102566

R_{SEI}	Solid electrolyte interphase resistance
R_{CT}	Charge-transfer resistance
C_{DL}	Double-layer capacitance
SEI	Solid electrolyte interphase
Φ_{xx}	Power spectral density of signal x
Φ_{xy}	Cross power spectral density of I/O signals x & y
γ_{xy}^2	Ordinary coherence of I/O signals x & y
PRS	Pseudo-random sequence
PRBS	Pseudo-random binary sequence
LTI	Linear and time-invariant
DFT	Discrete Fourier transform
BIBO	Bounded-input bounded-output
PSD	Power spectral density
CPSD	Cross power spectral density
KK	Kramers Kronig
SNR	Signal-to-noise ratio
NMC	Nickel-Manganese-Cobalt
CC	Constant current
CV	Constant voltage
m	Number of PRBS registers
t	Step time

This document is the pre-print version of the article:
Locorotondo, E., Cultrera, V., Pugi, L., Berzi, L., Pierini, M., Lutzemberger, G., 2021. Development of a battery real-time state of health diagnosis based on fast impedance measurements. Journal of Energy Storage 38, 102566.
https://doi.org/10.1016/j.est.2021.102566

a_i	PRBS gain factors
rem(x,2)	Modulo-2 operation
M	PRBS sample period
f_c	Clock frequency
f_s	Sampling frequency
L_f	Number of disjointed frames
N_f	Samples length of frames
$\sigma_{real,dataset}$	Standard deviation of real impedance dataset
$\sigma_{imag,dataset}$	Standard deviation of imaginary impedance dataset
$\sigma_{real,ins}$	Real impedance measurement uncertainty of the instrument
$\sigma_{imag,ins}$	Imaginary impedance measurement uncertainty of the instrument
G_0	Gain factor
Z	Impedance

This document is the pre-print version of the article:
Locorotondo, E., Cultrera, V., Pugi, L., Berzi, L., Pierini, M., Lutzemberger, G., 2021. Development of a battery real-time state of health diagnosis based on fast impedance measurements. Journal of Energy Storage 38, 102566.
https://doi.org/10.1016/j.est.2021.102566

I. INTRODUCTION

Lithium batteries (LIBs), with their high energy and power density, long cycle life, are widely used as energy storage units for electric and hybrid vehicles (EVs, HEVs). Currently, the automotive market is still dominated by vehicles powered with an internal combustion engine (ICE). However, the current market and technology trends are leading to the rapid growth of the diffusion of EVs and HEVs. The market share of ICE vehicles is predicted to fall from 99% in 2015 to 68% in 2030 [1]. Research works [2][3] agree on the growth estimation of LIB cells demand, driven predominantly but not exclusively by growth of automotive sector. According to [1] the limit of 100 $/kWh will be reached in 2025-2030 for several lithium-based batteries. Currently, there are several solutions to overcome this limit, e.g. developing battery chemistry with less costly new materials, adopting recycled materials (if available), increasing energy density per element, etc. The reuse of EV/HEV LIBs after their end-of-life (EOL), giving them a second life, has been considered one of the promising solutions to satisfy the battery demand of various sectors by extending use phase. Automotive LIBs are considered in EOL if its current capacity is at 85-80% of nominal capacity [4]-[8]. Despite a noticeable decrease in battery performance in EOL, as depicted in [4], second-life batteries are still expected to be capable of storing, delivering substantial energy and to meet the requirements of less-demanding applications, where reduced performances are still acceptable. Today, car manufacturers can also consider the second use option as an opportunity to expand their portfolio and enter in the stationary battery market.

In cooperation with utility companies, they are launching several pilot projects of battery second-life. The summary of these projects is presented in [5]. Therefore, several studies are focused on this topic: first investigations of the second-life battery from an economic, technical, and environmental viability perspective are carried out in [6][8]. A depth analysis of the aging evolution and impact of the battery in automotive applications, considering the impact on SOH of fast charging events or temperature conditions, is shown in [4][7]. Even if second life topics are stimulating a broad literature due to the need for diagnostics, standardization, and implementation in different contexts, diagnostics methods are a key need not only for such a life prolongation proposal but also to guarantee efficiency, safety and reliability of vehicle during first-life use. Amongst other reasons, it can be noted that accurate SOH assessment also improves SOC estimation, thus providing useful information for the vehicle user [9]; it has been demonstrated, also,

This document is the pre-print version of the article:
Locorotondo, E., Cultrera, V., Pugi, L., Berzi, L., Pierini, M., Lutzemberger, G., 2021. Development of a battery real-time state of health diagnosis based on fast impedance measurements. Journal of Energy Storage 38, 102566.
https://doi.org/10.1016/j.est.2021.102566

that certain aged cells can react in a worse to abuse evens in comparison with fresh ones [10], thus making diagnostics a matter of overall vehicle safety.

A. Literature review and contribution of the work

Hence, the battery state of health needs to be continuously monitored. Battery state of health (SOH), as defined in [11], is a metric to evaluate the aging level of batteries, which often includes capacity fade and/or power fade. Indeed, the capability of the battery to store energy (measured in current capacity Ah) and provide a certain power decreases over the battery life because of aging or unexpected events. Despite the importance of battery SOH analysis, it still does not a consensus in the literature on how the SOH should be determined. One of the most common SOH parameter assessment is the comparison of the current evaluated capacity with standard cycle respect to the initial capacity [11]. Recent control architectures include a new battery condition indicator similar to SOH, the so-called state of life (SOL). SOL evaluates the aging process due to the charging/discharging cycles performed during the normal operation of the storage system [12]. Instead, the SOH indicator monitors the battery health after anomalous or failure events, i.e. exceeding the peak current, overcharge, etc.

As previously mentioned, the initial level of SOH of second-life batteries, in terms of remaining capacity, is at SOH=85-80%, and the final value is considered at SOH=50% in [6][8], or SOH=60% in [13]. The development of improved battery SOH monitoring methods is still one of the main research topics in the field of LIBs in the automotive field, also concerning battery second use [11][14]. Generally, different approaches for SOH estimation through the use of model-based observers are proposed in the literature, such as Kalman filters [15][16], sliding mode observers[17], or least square filters [12][18]. These methods are usually based on voltage and current measurements, and adopt a battery equivalent circuit for model-based assessment. The model parameters should be adaptable to different operating conditions to ensure high accuracy on SOH estimation. A known disadvantage of these methods is the high computational efforts.

Data-driven methods, including statistical approach and machine learning methods, don't require accurate battery mathematical models, leading to a reduction of computational efforts [19]-[21]. However, an immense amount of measured data history is needed for a good SOH estimation accuracy.

This document is the pre-print version of the article:
Locorotondo, E., Cultrera, V., Pugi, L., Berzi, L., Pierini, M., Lutzemberger, G., 2021. Development of a battery real-time state of health diagnosis based on fast impedance measurements. Journal of Energy Storage 38, 102566.
https://doi.org/10.1016/j.est.2021.102566

Finally, electrochemical impedance spectroscopy (EIS) based methods are more diffused because they provide detailed information about the battery chemical-physical changes properties and different aging mechanisms [22]-[24]. Battery SOH monitoring based on EIS information is discussed in current research of secondary batteries [24]-[26] and other energy storage systems [27]-[29]. Concerning this promising method, there is a need to investigate the correlations between impedance information and battery SOH, the frequency range suitable for the analysis, and the implementation methods to make it easy to use. The aging mechanism can be studied using electrical circuit equivalent models, whose parameters are well identified fitting EIS data in a defined frequency band. Usually, the Randles circuit models [30][31] are used to fit impedance data.

Phenomena induced by cell structure and by its modification over time include: inductive behaviors, film formation, charge-transfer resistance and double-layer capacitance on the electrode-electrolyte interface, and diffusion processes in the active materials of the electrodes; according to literature, such phenomena can be investigated adopting EIS. Several research works in [22]-[36] confirm a monotonous increase of ohmic resistance ($\boldsymbol{R_{\Omega}}$) with battery degradation. To demonstrate the robust correlation between $\boldsymbol{R_{\Omega}}$ and SOH, experiments are carried out at different battery operating conditions: in [32][33] at different battery state of charge (SOC), considering fixed room temperature; in [34][35] at a different rate of discharge (C-rate); finally at different room temperature in [24][36]. Research work in [37] confirms a correlation between the increase of the resistance charge transfer ($\boldsymbol{R_{CT}}$) between electrodes with the aging cycles considering different temperature and SOC. In [38], the growth of the solid electrolyte interphase (SEI) film resistance ($\boldsymbol{R_{SEI}}$) is identified and correlated with battery SOH. Finally, the increase of double-layer capacitance ($\boldsymbol{C_{DL}}$) with aging is considered in [22][24]. The parameters cited are identified by using a non-linear best-fitting algorithm, for example, the most commonly used Levenberg-Marquardt method, which requires a high computational effort and an accurate choice of initial parameter values. Other research works [20][21] propose data-driven algorithms based on machine learning techniques to estimate battery SOH. Finally, research works in [39][40] present significant results since they correlate one single frequency response of battery with SOH: in [39], the increase of measured 100 mHz real battery impedance with aging is evaluated, testing four different lithium battery chemistry; in [40], the 316 Hz impedance shows negligible change respect to battery SOC and changes dramatically during overcharge. These last methods could be

This document is the pre-print version of the article:
Locorotondo, E., Cultrera, V., Pugi, L., Berzi, L., Pierini, M., Lutzemberger, G., 2021. Development of a battery real-time state of health diagnosis based on fast impedance measurements. Journal of Energy Storage 38, 102566.
https://doi.org/10.1016/j.est.2021.102566

considered an idea to perform a fast SOH diagnosis. However, for the development of an original method, it is fundamental to understand how to perform impedance spectroscopy identification with a simple test procedure; requirements of the application are also the adaptability to embedded systems and the reduced test time. Rapid and real-time EIS measurement methods are proposed in the literature in the last years. Authors in [41]-[48] propose different types of "broadband" current signal excitation for EIS identification in a set of frequencies at the same time. One of the most popular broadband excitation signals used is the multi-sine [41]-[43]: this signal is a sum of sines which frequency corresponds to the desired discrete set of frequency measured, with random phase. The multi-sine excitation approach offers more accurate EIS measurements [41][42], and various advantages in the detection of non-linear behaviors [43]. Pseudo-random sequence (PRS) signals are attractive alternatives, due to their low complexity, measurement time, and good accuracy [44]-[49]. The PRS family signals are periodic sequences that switch between two or three logic levels [44], so it shows a simple hardware implementation. Despite the multi-sine signal could provide accurate EIS measurements, the PRBS offers a more simple hardware implementation, which is fundamental for real-time battery state monitoring.

In conclusion, literature analysis shows an extensive investigation in literature of LIBs SOH monitoring during aging using EIS. Despite many authors in their research works have defined some condition indicators in the frequency domain to directly quantify SOH, the identification of these parameters has been obtained by high computational effort algorithms or with expensive facilities. This brief review shows that there are relatively few methods for monitoring battery SOH with EIS data adaptable in real-time applications. The main contribution of this work is the development of a new methodology to diagnose battery SOH by fast EIS measurements, addressed to embedded applications. This was achieved by realizing a low cost, low energy consumption, and low test time hardware PRBS generator. A large number of experimental EIS tests are performed at four EOL cells with different SOHs. Impedance measurements on cells under test are extracted performing EIS tests at various SOCs and different excitation current amplitudes. By experimental results, we will infer a noticeable correlation between SOH and impedance measurements. Indeed, we will determine frequency points (SOH frequencies) in which the impedance measurements dramatically change at different cell SOH. This was possible by clustering the set of cell impedances, measured at different SOH, in rectangular

This document is the pre-print version of the article:
Locorotondo, E., Cultrera, V., Pugi, L., Berzi, L., Pierini, M., Lutzemberger, G., 2021. Development of a battery real-time state of health diagnosis based on fast impedance measurements. Journal of Energy Storage 38, 102566.
https://doi.org/10.1016/j.est.2021.102566

areas defined in Nyquist diagrams (SOH clusters). The remainder of this paper is structured as follows. Section II describes the proposed method including requirements, indicators, and excitation signal characteristics. Section III describes the prototype testbed and shows measurements on new cells. Section IV includes the results obtained by aged cells testing and the data processing procedure.

II. A GENERAL PRINCIPLE FOR FAST EIS IDENTIFICATION

A. System Requirements

To perform EIS measurement, the battery system under test must be assumed and validated as LTI dynamic system. The linearity property can be assumed if the system is submitted to a small current excitation. However, a very small current perturbation causes noisy voltage response. Hence, it's important to select the input signal excitation with an appropriate amplitude, not too large because it would induce a non-linear response of the system and not too small because it would induce noisy responses. The time-invariant property can be assumed if the parameters, which define the battery system, are not changing with time. The main causes for time-variance in the battery system are the variations of temperature, SOC, current excitation (in terms of amplitude and sign), and finally aging. Moreover, if the battery voltage is in a transient state and has not reached its steady state, the system is considered as time-variant. The effects of time-variance in EIS measurements are noticeable in low frequency and are shown in [50][51]. Hence, to avoid impedance errors related to time-variant system behavior, sufficiently long rest time is required before the EIS test start, and, during the test, influence factors, especially temperature, must not change.

If the LTI assumptions are validated during the EIS test, battery impedance can be represented by the discrete-Fourier transform (DFT):

$$Z(k) = \sum_{n=0}^{N-1} z[n] e^{-j2\pi kn} \tag{1}$$

The variable $k \in$ [-1/2, 1/2] is the normalized frequency and N is the number of the harmonics. If the system is bounded-input bounded-output (BIBO) stable and the battery current input used for the EIS test is a periodic signal or a signal realization of a stationary stochastic process, the steady voltage response is the result of a stationary stochastic process. Hence, the impedance transfer function estimate is the ratio of two spectral estimates [52]:

This document is the pre-print version of the article:
Locorotondo, E., Cultrera, V., Pugi, L., Berzi, L., Pierini, M., Lutzemberger, G., 2021. Development of a battery real-time state of health diagnosis based on fast impedance measurements. Journal of Energy Storage 38, 102566.
https://doi.org/10.1016/j.est.2021.102566

$$Z(k) = \frac{\Phi_{vi}(k)}{\Phi_{ii}(k)} \tag{2}$$

Where: $\Phi_{ii}(k)$ is the battery current input power spectral density (PSD), and $\Phi_{vi}(k)$ is the cross-PSD (CPSD) of the battery voltage-current signal, computed by the voltage and current DFTs $V(k)$, and $I(k)$:

$$\begin{aligned} \Phi_{ii}(k) &= aI(k)I^*(k) \\ \Phi_{ii}(k) &= aV(k)I^*(k) \end{aligned} \tag{3}$$

Where *a* is a normalization factor, * denotes complex conjugation.

B. Quality Indicators

The validity of EIS measurements can be monitored by using different methods discussed in the literature [50]-[57]. As mentioned, the battery system's LTI property must be validated, and, given a current input, the observed output voltage response must not be noisy. One of the most common methods to check if the LTI property of a system is maintained is the Kramers-Kronig relation validity test [50][51]. The Kramers-Kronig relation dictates that real and imaginary parts are interdependent, presented in the Kramers-Kronig (KK) transform integrals [50], for a LTI and causal system. An interesting KK test algorithm is employed to validate the EIS measurements and it is presented in [51] and applied in [42]. The drawback of this method is the high computational effort. An alternative approach is the monitoring of the ordinary coherence value in frequency. Given the current input and voltage output PSD $\Phi_{ii}(k)$, $\Phi_{vv}(k)$, and the CPSD $\Phi_{vv}(k)$ ordinary coherence function [52]-[54] at the frequency *k* is defined as:

$$\gamma_{vi}^2(k) = \frac{|\Phi_{vi}(k)|^2}{\Phi_{ii}(k)\Phi_{vv}(k)} \tag{4}$$

This quality indicator, normalized between [0,1], can be viewed as the correlation coefficient between the input and output sequences at the frequency *k*. For an ideal LTI system, ordinary coherence is 1 in the frequency domain. If the input-output relation is completely unrelated, the coherence value is 0. If at a given frequency the coherence is greater than 0 and less than 1, the input-output relationship is not perfectly linear, or extraneous noises interfere in the output voltage measurement. The noise PSD $\Phi_{mm}(k)$ is related to coherence in [52] and evaluated according to the equation:

This document is the pre-print version of the article:
Locorotondo, E., Cultrera, V., Pugi, L., Berzi, L., Pierini, M., Lutzemberger, G., 2021. Development of a battery real-time state of health diagnosis based on fast impedance measurements. Journal of Energy Storage 38, 102566.
https://doi.org/10.1016/j.est.2021.102566

$$\Phi_{mm}(k) = (1 - \gamma_{vi}^2(k))\Phi_{vv}(k) \tag{5}$$

According to (5), given noise and output PSD, the output signal-to-noise ratio (SNR) can be estimated by ordinary coherence:

$$SNR(k) = \frac{\gamma_{vi}^2(k)}{1 - \gamma_{vi}^2(k)} \tag{6}$$

The ordinary coherence is a reliable quality indicator that can validate the impedance measurements, checking the LTI assumption for the battery system under test and the relative output SNR for each frequency measured *k*.

C. Excitation input signal: Pseudo-Random Binary Sequence (PRBS)

Broadband input signals are usually used for system identification in a wide frequency range, reducing test time. Three different classes of broadband signals have been considered in literature [52]-[54]:

- random signals (filtered Gaussian white noise and binary signals);
- transient signals (pulse or burst signals);
- periodic signals (multi-sine, pseudo-random sequences).

Periodic excitation signals are often used because they exhibit a lower crest-factor [52][53]. In this way, an accurate impedance estimation can be performed with low energy consumption. Finally, the spectral content of periodic signals can be optimized to prevent harmonic distortions due to leakage problems [54]. In this work, the pseudo-random binary sequence (PRBS) signal is chosen as the excitation input signal because it requires simple hardware implementation in comparison to a multi-sine approach or other periodic signals. This is a very important feature for a large scale industrial application. Denoted by the variable u_t, the PRBS is a deterministic and periodic sequence of length *N* which that switches between two logic levels {0,1}, and it is generated by the differential equation at step *t*:

$$u_t = \mathrm{rem}(a_1 u_{t-1} + \ldots + a_m u_{t-m}, 2) \tag{7}$$

Where rem(x, 2) is the modulo-2 addition on x [52], and a_i is the i −gain factor that takes integer values {0,1}, for $i = 1, \ldots, m$. The vector of past inputs $[u_{t-1}, u_{t-2}, \ldots, u_{t-n}]$ can only assume 2^m different values. Thus, the input signal u_t is periodic with a period of at most 2^m. In [52] it's proven that PRBS signal can have a maximum period of $M =$

This document is the pre-print version of the article:
Locorotondo, E., Cultrera, V., Pugi, L., Berzi, L., Pierini, M., Lutzemberger, G., 2021. Development of a battery real-time state of health diagnosis based on fast impedance measurements. Journal of Energy Storage 38, 102566.
https://doi.org/10.1016/j.est.2021.102566

$2^m - 1$ using an appropriate combination of gain factors vectors $[a_1, a_2, \dots, a_m]$. In [55], the PRBS signal (7) is generated considering a closed-loop shift register configuration of n bits in series, requiring a very simple hardware implementation. This binary sequence, if well designed, has properties similar to those of a white noise signal in the frequency domain. This is a clear advantage since it's possible to excite the system over a wide bandwidth, accelerating testing procedures.

The difference between the PRBS with maximum period length $M = 2^m - 1$ and white noise auto-covariance function decreases when the number of registers considered increases. Consequently, the difference between white noise and PRBS power spectral density (PSD) function decreases. In [52][53] we observe that the spectrum expression of PRBS of amplitude U is according to the following equation, at the angular frequency ω:

$$\Phi_{uu}(\omega) = U\frac{2\pi}{M}\sum_{k=1}^{M-1}\delta(\omega - \frac{2\pi k}{M}), \qquad 0 \le \omega < 2\pi \tag{8}$$

Where δ is the Dirac delta function. By (8), in the angular frequency region $[-\pi, \pi]$ there will be $M - 1$ frequency peaks. Therefore, PRBS shows a flatter PSD increasing the period, similar to the white noise signal. In this work, the number $m = 10$ of registers, hence a period of $M = 1023$ samples, is chosen for the PRBS generator used for the EIS test. Therefore, the PRBS with a period of $M = 1023$ samples has a band-limited flat PSD (8). We define the clock frequency f_c at which the input PRBS u_t (7) is synchronized. In [53] it is demonstrated that the PRBS presents an almost flat spectrum over the frequency band $[{}^{fc}/_{m}, fc]$, hence, in this work, over one frequency decade. Finally, the choice of a sampling frequency f_s about ten times the maximum frequency band is advisable for system identification in the frequency domain [52].

III. EXPERIMENTAL APPROACH AND VALIDATION EIS RESULTS

A. Laboratory setup and test procedure

The scheme of the proposed laboratory EIS test setup is depicted in Figure 1: the testing procedure, for system identification in the frequency domain, consists of exciting the battery in current with the periodic PRBS signal, using a low-cost programmable PRBS generator, discussed in the previous work [49]. An electronic circuit was designed to generate discharging PRBS current on the battery, shown on the left of Figure 1: the excitation signal is generated by

This document is the pre-print version of the article:
Locorotondo, E., Cultrera, V., Pugi, L., Berzi, L., Pierini, M., Lutzemberger, G., 2021. Development of a battery real-time state of health diagnosis based on fast impedance measurements. Journal of Energy Storage 38, 102566.
https://doi.org/10.1016/j.est.2021.102566

the microcontroller Texas F23879D, which, driving a power Mosfet, opens and closes the circuit at the clock frequency f_c.

The current PRBS signal generated has two current levels $\{0, I\}$, where I is controlled by the variable resistance R_{Load} inserted in series with the transistor. There is the possibility to conduct two different tests, switching manually the circuit selector shown in Figure 1: if the circuit is selected in 1, EIS test is performed on the battery under test (BUT); else, if the circuit is selected in 2, a reference sample impedance is inserted in series with the previous circuit. This last circuit will be used to validate impedance measurements and check the instrument accuracy. During the EIS test, battery voltage and current are measured and acquired by the DSpace MicroLabBox at a sampling frequency of 20 kHz, which is ten times the maximum EIS frequency band on which authors investigate for SOH diagnosis. Moreover, room and battery surface temperature are measured, with a sample time of 1s. When the EIS tests are finished, voltage and current data are processed to evaluate impedance (2) and coherence (4), following the approach explained as following.

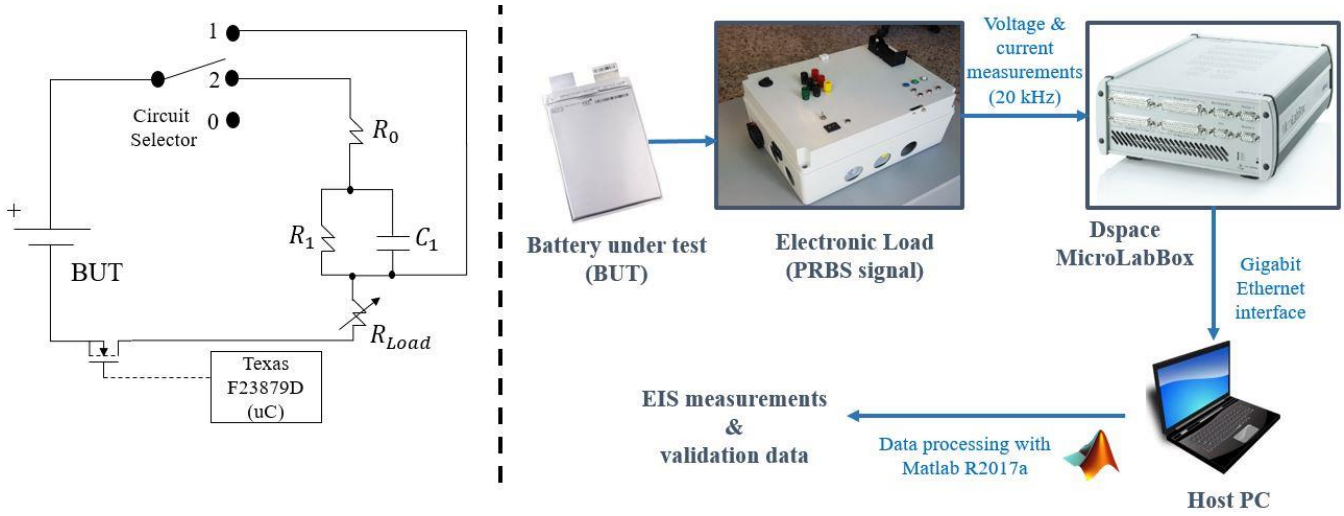

Figure 1. Laboratory battery EIS test setup on the right, electronic circuit of PRBS current generator on the left.

The experimental test protocol is illustrated in Figure 2: a charged battery (SOC=100%) is subjected to different EIS tests. Research works [22]-[38] investigated the battery SOH by EIS data in the frequency range approximately from mHz to kHz. In this work, battery impedance is evaluated in the frequency band [4,1600] Hz. In this specific range, research works [33]-[38] depicted that SOH characterizes the change of impedance curve, such as the change of ohmic, charge-transfer, and SEI resistance. Moreover, fast impedance measurements can be carried out in this range. As

This document is the pre-print version of the article:
Locorotondo, E., Cultrera, V., Pugi, L., Berzi, L., Pierini, M., Lutzemberger, G., 2021. Development of a battery real-time state of health diagnosis based on fast impedance measurements. Journal of Energy Storage 38, 102566.
https://doi.org/10.1016/j.est.2021.102566

mentioned, the PRBS, with $m = 10$ registers, has a flat spectrum in about one-decade frequency, based on the clock frequency. Therefore, the battery impedance spectrum will be estimated taking three consecutive PRBS tests at different clock frequency into consideration: 50, 500, and 4000 Hz. More details about PRBS are illustrated in Table 1. Tests are repeated considering various SOC and amplitude levels of PRBS current (C-rate), described in Table 2. Tests are performed starting from the highest SOC to the lower ones. Assuming that all EIS tests performed require less than 1% of battery SOC consumed, the battery is discharged at the rate of discharge of C/2 until it losses the remaining energy that is needed to reach the next desired SOC level. After a rest time of 1 h, to allow the battery voltage to reach its steady-state, EIS tests are carried out again. The experimental test is finished when the EIS tests are performed on the battery at the end of the discharge (about 2%). Based on battery voltage and current measurements, with a sample time of 20 kHz, battery impedance is evaluated in the frequency range [4,1600] Hz: we extracted 21 linearly spaced frequency points for every PRBS test at different clock frequency, as shown in Table 1. The guideline for appropriate bandwidth measured, by using the PRBS, is given in [53] equalling to $0.4f_c$. By results shown in Figure 3, we maintain this constraint for the 4 kHz PRBS, whereas we relax the last constraint considering the 50 and 500 Hz PRBS.

Table 1. Impedance measurement specifications

PRBS clock frequency (Hz)	Period time (s) (1023 samples)	Test duration time (s) (≥6-period repetitions)	Number of impedance measurements in the frequency	Frequency resolution (Hz)	Frequency band (Hz)
50	20.6	125	21	1.4	[4,40]
500	2.6	60	21	13.25	[45,400]
4000	0.256	10	21	82.50	[450,1600]

This document is the pre-print version of the article:
Locorotondo, E., Cultrera, V., Pugi, L., Berzi, L., Pierini, M., Lutzemberger, G., 2021. Development of a battery real-time state of health diagnosis based on fast impedance measurements. Journal of Energy Storage 38, 102566.
https://doi.org/10.1016/j.est.2021.102566

Table 2. EIS Test specifications performed on a single cell

Parameters change	Values	N. of test repetition
PRBS clock frequency	[50,500,4000] Hz	3
PRBS discharging current amplitude (C-rate)	[C/3,C/4,C5,C/6,C/20,C/25]	3
Battery SOC	[100,80,60,40,20,2] %	3

Impedance and coherence are estimated at different frequencies based on battery current PSD and voltage-current CPSD according to (2) and (4). These power spectral densities are estimated in frequencies applying the Welch periodograms [56]: voltage and current measurement signals are split into disjointed L_f frames of length N_f. Then, the voltage and current Fast Fourier transforms of every frames are computed according to (1), and multiplied by using Hamming window function. Hence the PSD and CPSD are computed according to (2), finally, the Welch periodogram estimator evaluates the PSD and CPSD computing the following mean value:

$$\Phi_{ii}(k) = \frac{a}{L_f}\sum_{j=1}^{L_f}\Phi_{ii,w,j}(k)$$
$$\Phi_{vi}(k) = \frac{a}{L_f}\sum_{j=1}^{L_f}\Phi_{vi,w,j}(k) \quad (9)$$

This document is the pre-print version of the article:
Locorotondo, E., Cultrera, V., Pugi, L., Berzi, L., Pierini, M., Lutzemberger, G., 2021. Development of a battery real-time state of health diagnosis based on fast impedance measurements. Journal of Energy Storage 38, 102566.
https://doi.org/10.1016/j.est.2021.102566

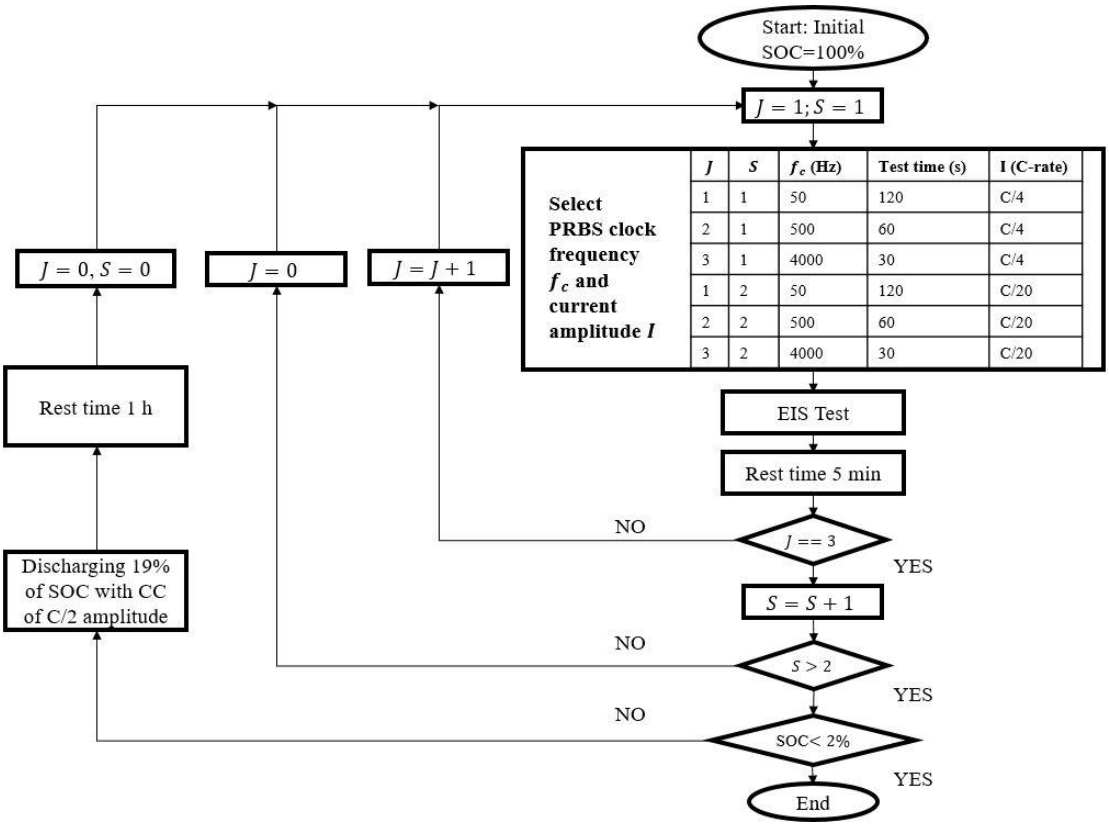

Figure 2. Experimental test protocol

This document is the pre-print version of the article:
Locorotondo, E., Cultrera, V., Pugi, L., Berzi, L., Pierini, M., Lutzemberger, G., 2021. Development of a battery real-time state of health diagnosis based on fast impedance measurements. Journal of Energy Storage 38, 102566.
https://doi.org/10.1016/j.est.2021.102566

B. Reference sample impedance circuit measurements

As mentioned in the previous section, the accuracy of EIS measurements is validated considering the electrical equivalent circuit given in Figure 1, switching the circuit selector in 2. Similar work was carried out in [57]. Referring to Figure 1, the circuit configuration, composed by the passive circuit elements R_0, R_1, C_1, defines the reference sample impedance. The circuit parameters are selected to describe a portion of a semi-circle. The resistance $R_0 = 1\ \Omega \pm 5\%$ is in series with RC group in parallel, composed by $R_1 = 50\ \text{m}\Omega \pm 5\%$ and $C_1 = 0.01\ \text{F} \pm 20\%$, considering a parasitic resistance $R_p = 10\ \text{m}\Omega \pm 5\%$ in series to capacitive element, given by the manufacturer. The battery under test is a Li[NiCoMn]O_2-based Cathode type (briefly called NMC) pouch cell, having a nominal capacity of 20 Ah [58]. For each PRBS signal at different clock frequency, impedance measurements are performed at various current amplitudes and different SOCs, shown in Table 2. This leads to a large number of EIS tests, in which impedance and coherence are computed. Impedance estimate results are compared with the theoretical impedance in the frequency range of [4,1600] Hz. The results demonstrated that measurements of sample impedance at different SOCs are very similar. Therefore, the authors will neglect this difference when discussing the validation of the sample impedance estimation. The corresponding estimated coherence, at different PRBS input signal, is depicted in Figure 3, whereas the estimated sample impedance is depicted in Figure 4. The estimated ordinary coherence is close to 1 all over the frequency band. Therefore, we infer by results in Figure 3 that the battery under test can be considered as LTI system, hence sample impedance can be well estimated. The results shown in Figure 4 demonstrate that the real and imaginary part of the sample impedance measurement of the laboratory test setup's accuracy slightly decreases when the clock frequency of the PRBS signal is increasing, especially during the test with a clock frequency $f_c = 4$ kHz. This is noticeable also observing the coherence estimated in Figure 3. Finally, the results of measured sample impedance had shown a well-known bias estimation error of 5%, which is corrected by authors. A similar bias estimation error is obtained in [57].

This document is the pre-print version of the article:
Locorotondo, E., Cultrera, V., Pugi, L., Berzi, L., Pierini, M., Lutzemberger, G., 2021. Development of a battery real-time state of health diagnosis based on fast impedance measurements. Journal of Energy Storage 38, 102566.
https://doi.org/10.1016/j.est.2021.102566

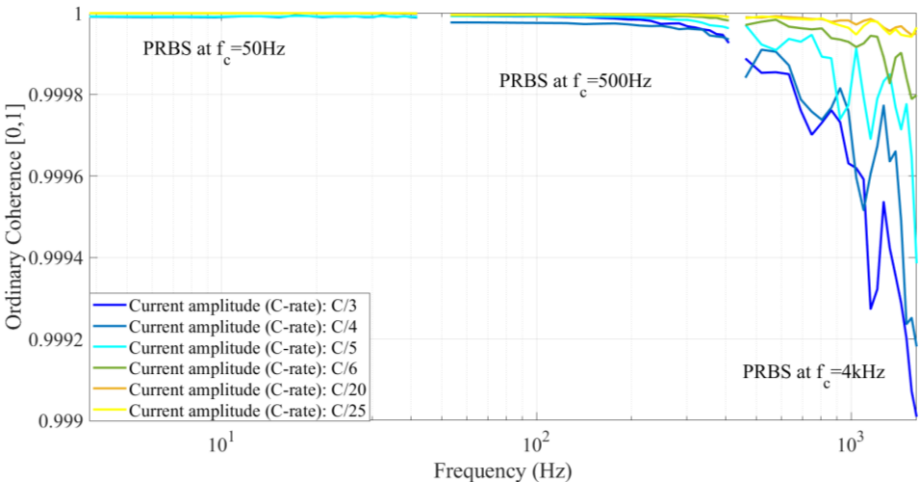

Figure 3. Ordinary coherence estimated using input PRBS signal excitation at different clock frequencies and current amplitudes (Battery is at 60% of SOC, estimation of sample impedance)

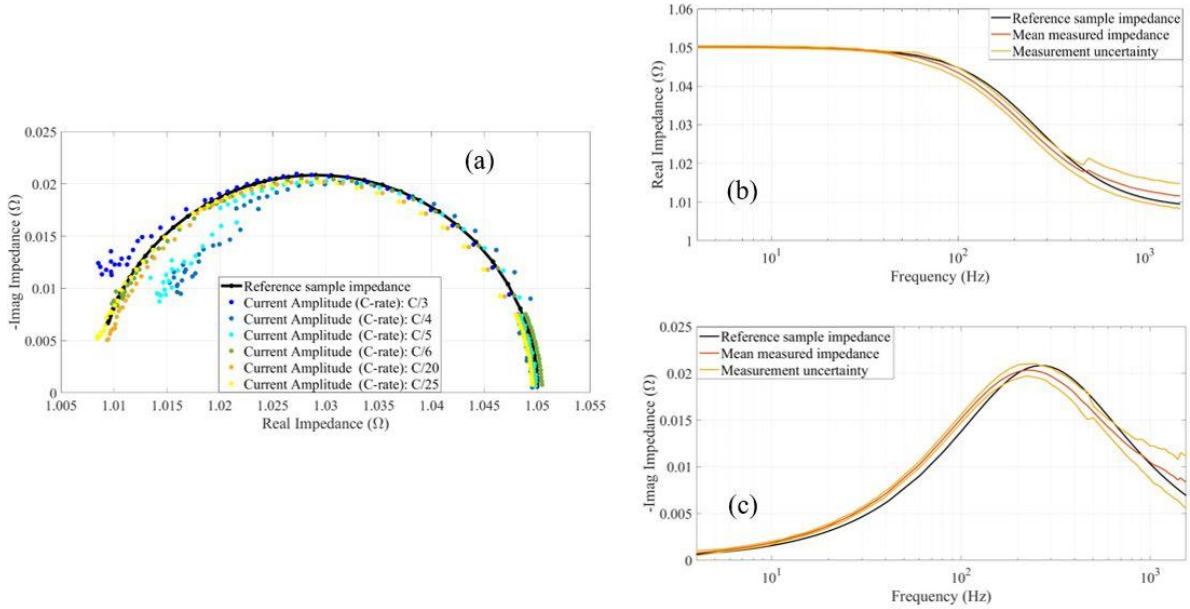

Figure 4. Reference impedance measurements using input PRBS signal excitation at different current amplitudes (Battery is at 60% of SOC, estimation of sample impedance): a) Nyquist plot, b) Real impedance and c) – Imaginary impedance vs frequency

This document is the pre-print version of the article:
Locorotondo, E., Cultrera, V., Pugi, L., Berzi, L., Pierini, M., Lutzemberger, G., 2021. Development of a battery real-time state of health diagnosis based on fast impedance measurements. Journal of Energy Storage 38, 102566.
https://doi.org/10.1016/j.est.2021.102566

C. *New cell impedance measurements*

The battery impedance estimation is performed considering the equivalent circuit given in Figure 1, switching the circuit selector in 1. In this section, the NMC new cell is under test. EIS results are depicted in Figure 5.

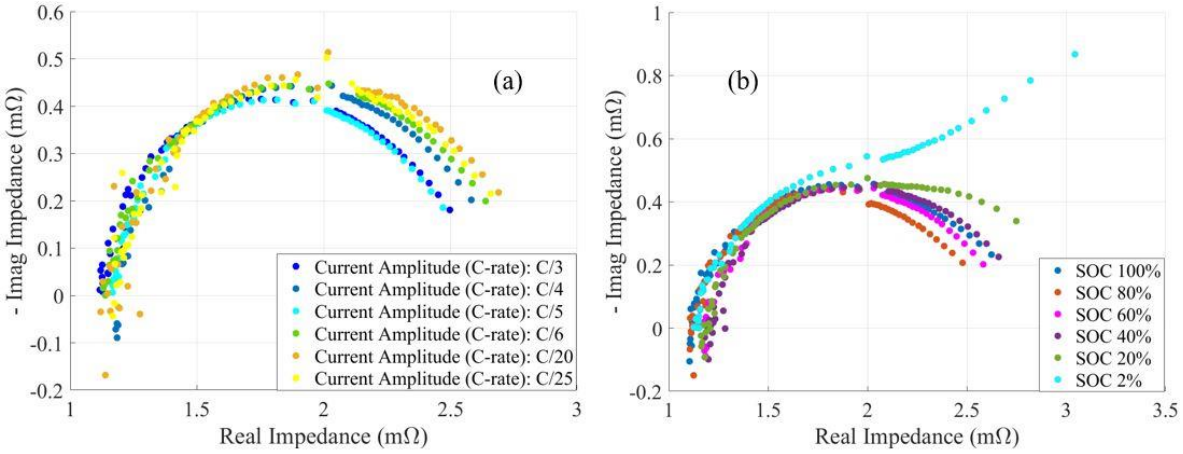

Figure 5. EIS measurements using input PRBS signal at different a) current amplitudes (fixed SOC 60%) and b) SOCs (fixed current amplitude C/4)

We notice that all the battery impedance measurements are about in the interval of 2 mΩ, in the real part, and 0.5 mΩ, in the imaginary part. These intervals are shorter than the sample impedance measurements in the previous experiment, hence, the external noise sources could strongly affect the EIS measurements, decreasing the ordinary coherence. As just mentioned, noise contributions can be minimized by increasing the excitation power when an improved coherence is reached, as shown in Figure 6. The battery impedance curves measurements given in Figure 5 (on the left) show a slight difference when changing the current discharging amplitude. Instead, results given in Figure 5 (on the right) show that there is a drastic change of impedance curve when the battery is at the end of discharge, confirmed also in [33][35].

IV. SOH DIAGNOSIS BASED ON EIS DATA

A. *Testing cell at different state of healths*

To detect battery SOH using EIS tests, five pouch NMC cells, of the same manufacturer, were tested at different SOHs. In this work, battery SOH is considered by the variation of battery capacity compared to its ideal condition, in this case, 20 Ah. One of the five cells under test is fresh and therefore considered as at the beginning of life (new cell). The other four cells have been cycled until they reached EOL for automotive application, and beyond. Results of the

This document is the pre-print version of the article:
Locorotondo, E., Cultrera, V., Pugi, L., Berzi, L., Pierini, M., Lutzemberger, G., 2021. Development of a battery real-time state of health diagnosis based on fast impedance measurements. Journal of Energy Storage 38, 102566.
https://doi.org/10.1016/j.est.2021.102566

capacity test, which denote the current battery SOH, are shown in Table 3. The EOL cells were subjected to 4 different cycle life test, composed by constant-current (CC), at current amplitude C/2, and, finally, constant-voltage (CV) charging; followed by discharging phases (C/2), interspersed with pauses, at a room temperature of 35°C [59]. Cycle life tests were carried out in ENEA research center from 2015 to 2018. More details about cycle life tests and cell history are shown in [12][59]. Afterwards, the cells have not been used for about 2 years, and have been stored in the same conditions (in a not thermally controlled environment).

Table 3. Battery cells at different SOHs

Battery n.	Last capacity estimated (Ah)	State of Health (%)
#0	20	100
#3	16	80
#4	17	85
#5	12	60
#8	10	50

B. Battery impedance data-set

The laboratory setup, shown in Figure 1, was used to perform EIS in the frequency band [4,1600] Hz, using the PRBS signal excitation in current at three different clock frequencies. For each PRBS test, we extract 21 impedance measurements for each different clock frequency PRBS in the band specified in Table 1. To investigate if there is a robust correlation between impedance information and SOH, we measure battery impedance at various operating conditions. According to Table 2, EIS is executed at six different battery SOC, and two different PRBS discharging current amplitudes, exactly at C-rate C/4, and C/20. To test the laboratory setup's repeatability, tests were repeated three times. Summarizing, we performed a large number of EIS experiments for each cell, collecting a large number of impedance measurements. Results of the repeatability test had shown a very negligible variation of battery impedance estimation, then, the mean impedance value will be shown in this work whereas the authors will discuss of EIS data set and data clustering. Finally, the data set of each cell under test is composed of 756 impedance measurements in the

This document is the pre-print version of the article:
Locorotondo, E., Cultrera, V., Pugi, L., Berzi, L., Pierini, M., Lutzemberger, G., 2021. Development of a battery real-time state of health diagnosis based on fast impedance measurements. Journal of Energy Storage 38, 102566.
https://doi.org/10.1016/j.est.2021.102566

defined frequency band. Concerning a single frequency investigated, the data-set is composed of 12 impedance measurements, at various SOCs, and rate of discharge. Results obtained by ordinary coherence for EOL cells are shown in Figure 6. We infer that there is a slight increase in ordinary coherence with SOH decreasing. A complete view of the impedance points extracted for every cell is depicted in Figure 7. It's noticeable, as mentioned in the literature, the shift on the right of the impedance curve, which means an increase of the real part of battery impedance, i.e. the increase of the ohmic resistance, a fact in accordance with other literature observations [22]-[36]. Moreover, the increase of the semi-ellipses arcs with aging is noticeable in Figure 7, which means the increase of the charge transfer resistance [37] and the SEI resistance [38] with aging. We observe in Figure 7 that the impedance curve of the new cell is an order of amplitude different respect to the EOL cells. Moreover, the new cell is completely disjointed with the EOL cell impedance curves. Therefore, using the EIS test, it is simple to distinguish a new cell from the EOL cell by performed measurements of impedance.

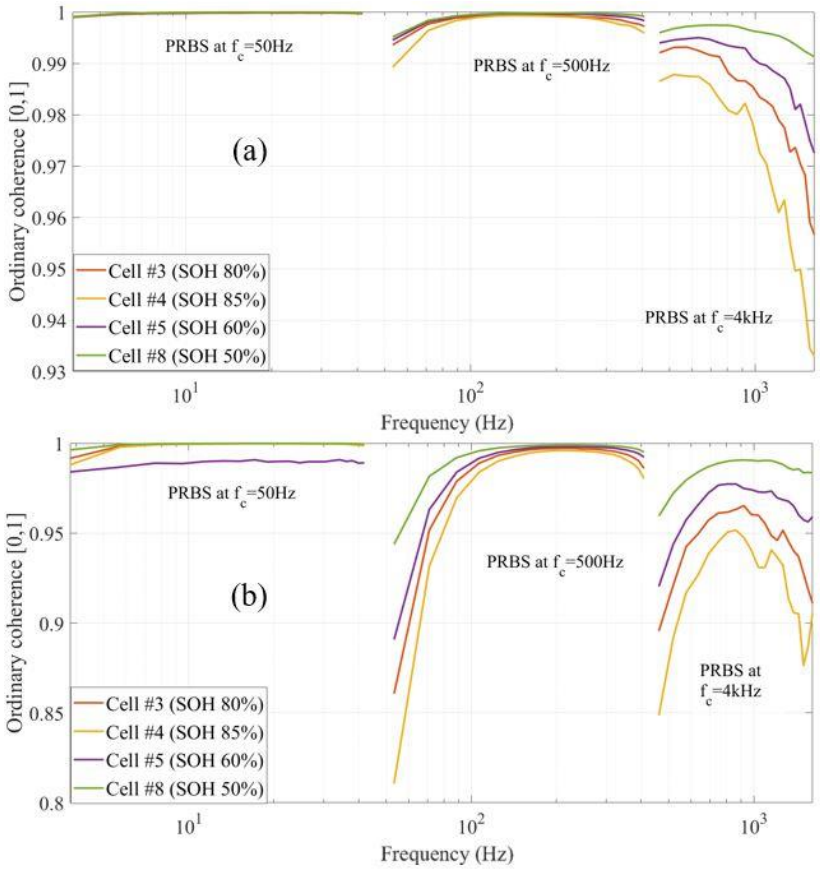

This document is the pre-print version of the article:
Locorotondo, E., Cultrera, V., Pugi, L., Berzi, L., Pierini, M., Lutzemberger, G., 2021. Development of a battery real-time state of health diagnosis based on fast impedance measurements. Journal of Energy Storage 38, 102566.
https://doi.org/10.1016/j.est.2021.102566

Figure 6. Mean ordinary coherence estimated during EIS test for different cells using the excitation PRBS with discharging current amplitude of a) C/4, b) C/20

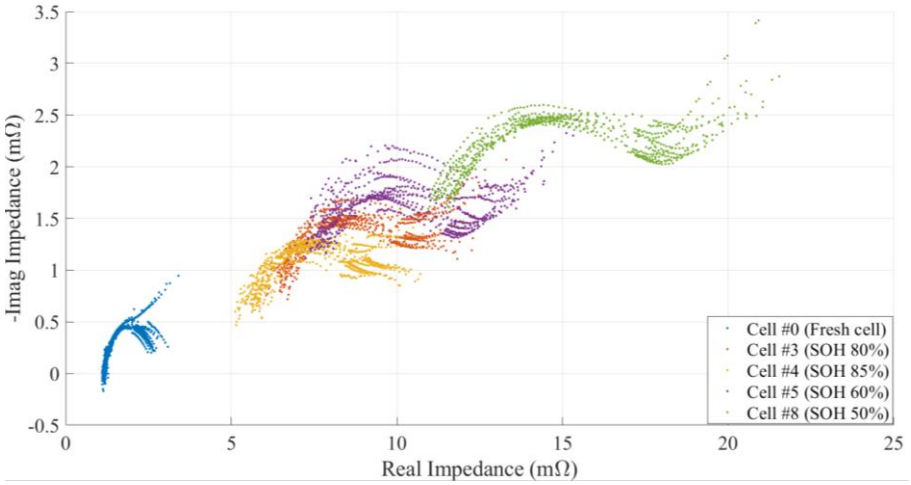

Figure 7. Battery EIS measurement data-set in the frequency band [4,1600] Hz, at various SOCs and PRBS discharging current amplitudes

C. Data clustering

Diagnosis and identification of the battery SOH are performed by using the EIS test. The question remains as to whether there are frequency points in which battery impedance is evaluated in a well-disjointed range of measurement, carried out at various operating conditions, such as SOCs and current C-rate. We infer by Figure 7 that, in some frequency points, there is the possibility to cluster disjointed area of impedance measurements in the Nyquist diagram. An example is shown in Figure 8, considering the frequency measurement of 88.8 Hz. For every frequency, all the SOH area clusters are defined in the Nyquist diagram enclosing the 12 impedance measurements, by using rectangle geometry. Every rectangle's edge is defined by the maximum and the minimum value of the real and imaginary part of impedance measured, adding or subtracting an external factor:

$$\sigma(j\omega) = G_0[(\sigma_{real,dataset} + \sigma_{imag,dataset}) + (\sigma_{real,ins} + j\sigma_{imag,ins})] \quad (10)$$

The value of the external factor corresponds to the sum of the maximum variation (std) observed by the impedance measurements in all the single frequency clusters $(\sigma_{real,dataset} + j\sigma_{imag,ins})$, and of the uncertainty $(\sigma_{real,ins} + j\sigma_{imag,ins})$ of the laboratory setup shown in Figure 4, relative to the diameter of the reference sample impedance. The gain factor G_0=0.5 is considered in (10).

This document is the pre-print version of the article:
Locorotondo, E., Cultrera, V., Pugi, L., Berzi, L., Pierini, M., Lutzemberger, G., 2021. Development of a battery real-time state of health diagnosis based on fast impedance measurements. Journal of Energy Storage 38, 102566.
https://doi.org/10.1016/j.est.2021.102566

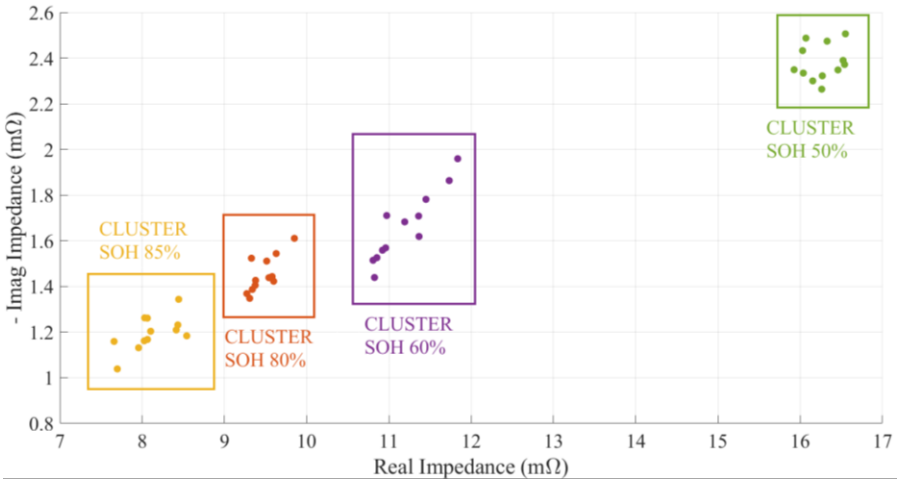

Figure 8. Battery EIS measurement data clustering at frequency 88.8 Hz

V. RESULTS & DISCUSSION

A. Detection of SOH frequencies

In section II, we have demonstrated that battery impedance can be fast measured by using the low-cost PRBS generator shown in Figure 1. A large number of EIS experiments are performed on four EOL cells and described in section III. By clustering the impedance measurements in rectangular areas, we can detect the SOH frequencies. In these frequencies the SOH area clusters are disjointed, hence, they are candidates as reliable SOH indicators. As noticeable in Figure 8, the SOH clusters are disjointed if and only if there is no intersection between real-axis or between imaginary-axes of rectangles. The EIS measurements were carried out at different battery operating conditions, hence SOC variations [0,100] % and PRBS current C-rate amplitudes variations (C/4, C/20). The SOH clusters are defined for each frequency measured and cited in Table 2. The results obtained have demonstrated that it is not possible to highlight a SOH frequency in which the imaginary-axes of SOH clusters are disjointed and real-axes not. Indeed, as demonstrated by some research work in literature [22][24], the real impedance measurement is usually exploited to detect battery aging defined. The total number of SOH frequencies detected is 3 than 61 frequencies measured, in the band [4÷1600] Hz. The SOH frequencies and the corresponding SOH clusters are shown in Table 4 and Figure 9. We infer that there is a noticeable variation of battery impedance measurement at different SOH in the three frequencies measured in the band [53.8÷88.8] Hz, by using the 500 Hz PRBS. In this first result, we consider all the EIS experiments. In the next section, we will detect larger and new SOH frequency bands by filtering experimental data.

This document is the pre-print version of the article:
Locorotondo, E., Cultrera, V., Pugi, L., Berzi, L., Pierini, M., Lutzemberger, G., 2021. Development of a battery real-time state of health diagnosis based on fast impedance measurements. Journal of Energy Storage 38, 102566.
https://doi.org/10.1016/j.est.2021.102566

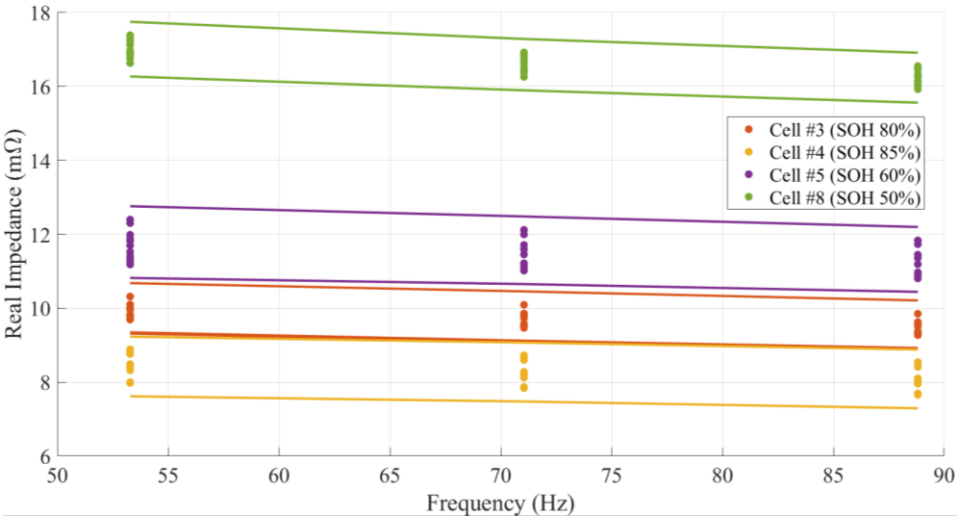

Figure 9. Detection of the SOH frequencies, illustrating the real impedance measurements for the different aged cells enclosed by disjointed area clusters

B. Detection of SOH frequencies filtering data

SOH cluster's areas change when filtering the EIS experiment. Hence, the number of SOH frequencies detected could be changed. We have analysed and defined the clusters considering 4 different types of EIS experiment filtering:

- Case (a): EIS experiments in the SOC interval [20÷80] % (impedance measurements at extreme of SOC values are less reliable).
- Case (b): EIS experiments with PRBS current of discharge amplitude of C/20 (response with lower currents).
- Case (c): EIS experiments with PRBS current of discharge amplitude of C/4 (response with higher currents)
- Case (d): EIS experiments in the SOC interval [20÷80] %, with PRBS current of discharge amplitude of C/4 (best condition, high current, reliable SOC values).

The SOH frequencies detected, filtering data according to the four different cases study are shown in Table 4. The corresponding SOH clusters obtained in the SOH frequencies are shown in Figure 10. Results obtained in the case (a) confirm the detection of the same SOH frequency band observed in the previous analysis. Moreover, a new frequency band is detected: [4÷24] Hz, measured by using the 50 Hz PRBS. This last results confirm that, as cited in the literature [24], and shown in Figure 5, impedance measurements drastically change their value when the EIS test is performed at the extreme of battery SOC. Hence, removing these data, impedance measurements are closes to them. Referring to the

This document is the pre-print version of the article:
Locorotondo, E., Cultrera, V., Pugi, L., Berzi, L., Pierini, M., Lutzemberger, G., 2021. Development of a battery real-time state of health diagnosis based on fast impedance measurements. Journal of Energy Storage 38, 102566.
https://doi.org/10.1016/j.est.2021.102566

case (b), the SOH frequency band becomes larger ([54, 125] Hz) than the case (a). Nevertheless, the SOH frequency band [4÷24] Hz disappears, because we consider the impedance measurements at the extreme of SOC.

Generally, the impedances measured in the cases (a) and (b) are not very close to them. Indeed the power spectral of PRBS excitation signal with C/20 current amplitude is low, hence, voltage output observed is more affected by noise, decreasing the coherence spectra results, as shown in Figure 6. Hence impedance measurements are less reliable. This deduction is confirmed by the case (c): increasing the power of the PRBS excitation signal until C/3, the impedance measurements in the SOH frequencies, are very close to them, as shown in Figure 10. We infer that all frequencies measured by using 50 Hz and 500 Hz PRBS become a good indicator of battery SOH. Moreover, the new SOH frequency band [461÷922] Hz extracted by the 4 kHz PRBS is detected. Finally, results obtained in the case (d) demonstrate that all the frequency measured become as SOH frequencies. This last case, considering only the impedance measurements at the SOC in [20÷80] % and high current excitation, could be an acceptable constraint for EIS measurements in real-time applications. Usually, battery packs are used with a reduced DOD (not 100%), prolonging their lifetime. Moreover, all the EIS tests consumed less than 1% of battery SOC. As it is well observable from Figure 8-10, the clustering of the impedance measurements allows us to determine the SOH directly. The experimental EIS tests allowed us to define each SOH cluster region in an appropriate range of impedance measurement (real or imaginary part). For every single SOH frequency detected, the SOH clusters are disjointed between them. Hence, we can assess SOH with low computational efforts by performing the fast EIS test in one of the SOH frequency bands detected.

This document is the pre-print version of the article:
Locorotondo, E., Cultrera, V., Pugi, L., Berzi, L., Pierini, M., Lutzemberger, G., 2021. Development of a battery real-time state of health diagnosis based on fast impedance measurements. Journal of Energy Storage 38, 102566.
https://doi.org/10.1016/j.est.2021.102566

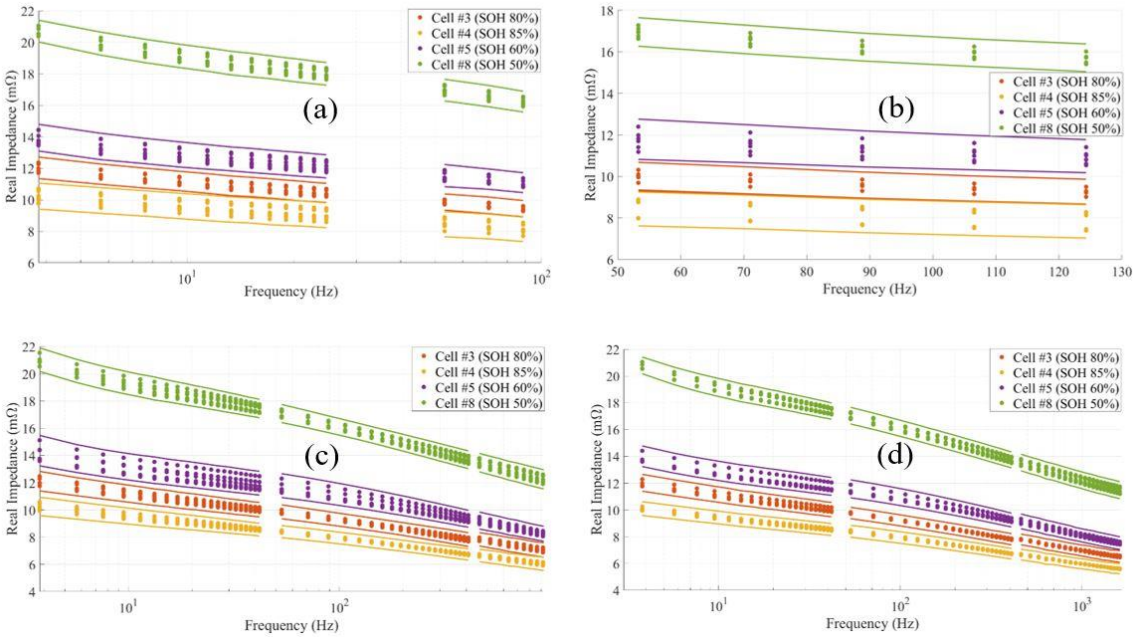

Figure 10. Detection of the SOH frequencies, filtering data: (a) SOC in [20÷80] %; (b) fixed C-rate C/20; (c) fixed C-rate C/4; (d) SOC in [20÷80] % and fixed C-rate C/4

This document is the pre-print version of the article:
Locorotondo, E., Cultrera, V., Pugi, L., Berzi, L., Pierini, M., Lutzemberger, G., 2021. Development of a battery real-time state of health diagnosis based on fast impedance measurements. Journal of Energy Storage 38, 102566.
https://doi.org/10.1016/j.est.2021.102566

Table 4. Detection of the SOH frequencies considering different battery impedance data set

Impedance data set	Number of impedance measured in single-frequency	50 Hz PRBS		500 Hz PRBS		4 kHz PRBS	
		Frequency band (Hz)	SOH frequency band (Hz)	Frequency band (Hz)	SOH frequency band (Hz)	Frequency band (Hz)	SOH frequency band (Hz)
SOC [0÷100] %, Current amplitude PRBS C/4,C/20	36	[4÷40]	/	[53÷400]	[53,89]	[450÷1600]	/
SOC [20÷80] %, Current amplitude PRBS C/4,C/20	24	[4÷40]	[4÷24]	[53 ÷400]	[53 ÷89]	[450÷1600]	/
SOC [0÷100] %, Current amplitude PRBS C/20	18	[4÷40]	/	[53 ÷400]	[53 ÷125]	[450÷1600]	/
SOC [0÷100] %, Current amplitude PRBS C/4	18	[4÷40]	[4÷40]	[53 ÷400]	[53 ÷400]	[450÷1600]	[450,922]
SOC [20÷80] %, Current amplitude PRBS C/4	12	[4÷40]	[4÷40]	[53 ÷400]	[53 ÷400]	[450÷1600]	[450÷1600]

CONCLUSIONS

The electrochemical impedance spectroscopy (EIS) is a powerful method to investigate the state of lithium batteries. The proposed methodology is applied to a specific benchmark cell but it should be extended almost to any kind of energy storage system. In this work, authors not only explore the feasibility of the proposed approach but evaluate how specific

test parameters/specifications can affect the quality of performed evaluations. The chosen excitation signal plays a key role in defining the complexity and consequently the industrial applicability of proposed spectroscopy techniques.

The PBRS excitation signal has proven, in this work, to be a good solution for possible industrial implementation. Authors have experimentally verified that it's possible to generate the PRBS signal with relatively cheap hardware to perform battery impedance measurements that in literature are typically obtained with far more expensive and specialized equipment.

Preliminary experimental activities have been performed both on a reference sample impedance to assess the capability of the system to identify a generic impedance and to propose a simple calibration method for field or industrial related activities.

Finally, EIS tests are performed on four end-of-life (EOL) automotive cells, ready for possible second use in less-demanding applications. Results confirm the existence of specific frequency bands candidate as a reliable and robust indicator of the state of health, depending on the operating conditions of the battery. Clustering impedance measurements in SOH regions allowed to detect these frequencies and correlate SOH with cell impedance with low computational efforts.

More generally, the study of second-life batteries is the only one of the many possible applications of a method that has proven to be fast and reliable. This novel method should be extended to many other applications in which a fast and accurate diagnostic of cell state of health has to be performed.

REFERENCES

[1] Berckmans, G., Messagie, M., Smekens, J., Omar, N., Vanhaverbeke, L., & Van Mierlo, J. (2017). Cost projection of state of the art lithium-ion batteries for electric vehicles up to 2030. Energies, 10(9), 1314.

[2] Blomgren, G. E. (2016). The development and future of lithium ion batteries. Journal of The Electrochemical Society, 164(1), A5019.

[3] Lebedeva, N., Persio, F.D., Boon-Brett, L., 2017. Lithium ion battery value chain and related opportunities for Europe (No. EUR 28534 EN). Publications Office of the European Union, Luxembourg.

This document is the pre-print version of the article:
Locorotondo, E., Cultrera, V., Pugi, L., Berzi, L., Pierini, M., Lutzemberger, G., 2021. Development of a battery real-time state of health diagnosis based on fast impedance measurements. Journal of Energy Storage 38, 102566. https://doi.org/10.1016/j.est.2021.102566

[4] Omar, N., Monem, M. A., Firouz, Y., Salminen, J., Smekens, J., Hegazy, O., ... & Van Mierlo, J. (2014). Lithium iron phosphate based battery–assessment of the aging parameters and development of cycle life model. Applied Energy, 113, 1575-1585.

[5] Bobba, S., Podias, A., Di Persio, F., Messagie, M., Tecchio, P., Cusenza, M. A., ... & Pfrang, A. (2018). Sustainability Assessment of Second Life Application of Automotive Batteries (SASLAB). JRC Exploratory Research (2016-2017 Final report).

[6] Neubauer, J., & Pesaran, A. (2011). The ability of battery second use strategies to impact plug-in electric vehicle prices and serve utility energy storage applications. Journal of Power Sources, 196(23), 10351-10358.

[7] Groenewald, J., Grandjean, T., & Marco, J. (2017). Accelerated energy capacity measurement of lithium-ion cells to support future circular economy strategies for electric vehicles. Renewable and Sustainable Energy Reviews, 69, 98-111.

[8] Martinez-Laserna, E., Gandiaga, I., Sarasketa-Zabala, E., Badeda, J., Stroe, D. I., Swierczynski, M., & Goikoetxea, A. (2018). Battery second life: Hype, hope or reality? A critical review of the state of the art. Renewable and Sustainable Energy Reviews, 93, 701-718.

[9] Shen, P., Ouyang, M., Lu, L., Li, J., Feng, X., 2018. The Co-estimation of State of Charge, State of Health, and State of Function for Lithium-Ion Batteries in Electric Vehicles. IEEE Transactions on Vehicular Technology 67, 92–103. https://doi.org/10.1109/TVT.2017.2751613

[10] Friesen, A., Horsthemke, F., Mönnighoff, X., Brunklaus, G., Krafft, R., Börner, M., Risthaus, T., Winter, M., Schappacher, F.M., 2016. Impact of cycling at low temperatures on the safety behavior of 18650-type lithium ion cells: Combined study of mechanical and thermal abuse testing accompanied by post-mortem analysis. Journal of Power Sources 334, 1–11. https://doi.org/10.1016/j.jpowsour.2016.09.120

[11] Berecibar, M., Gandiaga, I., Villarreal, I., Omar, N., Van Mierlo, J., & Van den Bossche, P. (2016). Critical review of state of health estimation methods of Li-ion batteries for real applications. Renewable and Sustainable Energy Reviews, 56, 572-587.

This document is the pre-print version of the article:
Locorotondo, E., Cultrera, V., Pugi, L., Berzi, L., Pierini, M., Lutzemberger, G., 2021. Development of a battery real-time state of health diagnosis based on fast impedance measurements. Journal of Energy Storage 38, 102566.
https://doi.org/10.1016/j.est.2021.102566

[12] Ceraolo, M., Giglioli, R., Lutzemberger, G., Langroudi, M. M., Poli, D., Andrenacci, N., & Pasquali, M. (2018, June). Experimental analysis of NMC lithium cells aging for second life applications. In 2018 IEEE International Conference on Environment and Electrical Engineering and 2018 IEEE Industrial and Commercial Power Systems Europe (EEEIC/I&CPS Europe) (pp. 1-6). IEEE.

[13] Saez-de-Ibarra, A., Martinez-Laserna, E., Stroe, D. I., Swierczynski, M., & Rodriguez, P. (2016). Sizing study of second life Li-ion batteries for enhancing renewable energy grid integration. IEEE Transactions on Industry Applications, 52(6), 4999-5008.

[14] Waag, W., Fleischer, C., & Sauer, D. U. (2014). Critical review of the methods for monitoring of lithium-ion batteries in electric and hybrid vehicles. Journal of Power Sources, 258, 321-339.

[15] Watrin, N., Blunier, B., & Miraoui, A. (2012, June). Review of adaptive systems for lithium batteries state-of-charge and state-of-health estimation. In 2012 IEEE Transportation Electrification Conference and Expo (ITEC) (pp. 1-6). IEEE.

[16] Chen, Z., Mi, C. C., Fu, Y., Xu, J., & Gong, X. (2013). Online battery state of health estimation based on Genetic Algorithm for electric and hybrid vehicle applications. Journal of Power Sources, 240, 184-192.

[17] Kim, I. S. (2009). A technique for estimating the state of health of lithium batteries through a dual-sliding-mode observer. IEEE Transactions on Power Electronics, 25(4), 1013-1022.

[18] Locorotondo, E., Pugi, L., Berzi, L., Pierini, M., & Pretto, A. (2018, June). Online State of Health Estimation of Lithium-Ion Batteries Based on Improved Ampere-Count Method. In 2018 IEEE International Conference on Environment and Electrical Engineering and 2018 IEEE Industrial and Commercial Power Systems Europe (EEEIC/I&CPS Europe) (pp. 1-6). IEEE.

[19] Lin, H. T., Liang, T. J., & Chen, S. M. (2012). Estimation of battery state of health using probabilistic neural network. IEEE Transactions on Industrial Informatics, 9(2), 679-685.

[20] Lei, Y., Li, N., Guo, L., Li, N., Yan, T., & Lin, J. (2018). Machinery health prognostics: A systematic review from data acquisition to RUL prediction. Mechanical Systems and Signal Processing, 104, 799-834.

This document is the pre-print version of the article:
Locorotondo, E., Cultrera, V., Pugi, L., Berzi, L., Pierini, M., Lutzemberger, G., 2021. Development of a battery real-time state of health diagnosis based on fast impedance measurements. Journal of Energy Storage 38, 102566.
https://doi.org/10.1016/j.est.2021.102566

[21] Khaleghi, S., Firouz, Y., Van Mierlo, J., & Van den Bossche, P. (2019). Developing a real-time data-driven battery health diagnosis method, using time and frequency domain condition indicators. Applied Energy, 255, 113813.

[22] Tröltzsch, U., Kanoun, O., & Tränkler, H. R. (2006). Characterizing aging effects of lithium ion batteries by impedance spectroscopy. Electrochimica acta, 51(8-9), 1664-1672.

[23] Raijmakers, L. H. J., Danilov, D. L., Van Lammeren, J. P. M., Lammers, M. J. G., & Notten, P. H. L. (2014). Sensorless battery temperature measurements based on electrochemical impedance spectroscopy. Journal of Power Sources, 247, 539-544.

[24] Waag, W., Käbitz, S., & Sauer, D. U. (2013). Experimental investigation of the lithium-ion battery impedance characteristic at various conditions and aging states and its influence on the application. Applied energy, 102, 885-897.

[25] Nguyen, T. T., Tran, V. L., & Choi, W. (2014, June). Development of the intelligent charger with battery State-Of-Health estimation using online impedance spectroscopy. In 2014 IEEE 23rd International Symposium on Industrial Electronics (ISIE) (pp. 454-458). IEEE.

[26] Stroe, D. I., Knap, V., Swierczynski, M., & Schaltz, E. (2018). Electrochemical impedance spectroscopy-based electric circuit modeling of lithium–sulfur batteries during a discharging state. IEEE Transactions on Industry Applications, 55(1), 631-637.

[27] Yang, H., Yoshio, M., Isono, K., & Kuramoto, R. (2002). Improvement of commercial activated carbon and its application in electric double layer capacitors. Electrochemical and Solid State Letters, 5(6), A141.

[28] Escalante-García, I. L., Wainright, J. S., Thompson, L. T., & Savinell, R. F. (2014). Performance of a non-aqueous vanadium acetylacetonate prototype redox flow battery: examination of separators and capacity decay. Journal of The Electrochemical Society, 162(3), A363.

[29] Darowicki, K., Janicka, E., Mielniczek, M., Zielinski, A., Gawel, L., Mitzel, J., & Hunger, J. (2019). The influence of dynamic load changes on temporary impedance in hydrogen fuel cells, selection and validation of the electrical equivalent circuit. Applied Energy, 251, 113396.

This document is the pre-print version of the article:
Locorotondo, E., Cultrera, V., Pugi, L., Berzi, L., Pierini, M., Lutzemberger, G., 2021. Development of a battery real-time state of health diagnosis based on fast impedance measurements. Journal of Energy Storage 38, 102566.
https://doi.org/10.1016/j.est.2021.102566

[30] F. Berthier, J.P Diard, R. Michel, "Distinguishability of equivalent circuits containing CPEs: Part I. Theoretical part." Journal of Electroanalytical Chemistry, 510(1-2), 1-11, 2001.

[31] Locorotondc, E., Pugi, L., Berzi, L., Pierini, M., Scavuzzc, S., Ferraris, A., ... & Carello, M. (2019, September). Modeling and simulation of Constant Phase Element for battery Electrochemical Impedance Spectroscopy. In 2019 IEEE 5th International forum on Research and Technology for Society and Industry (RTSI) (pp. 225-230). IEEE.

[32] Stroe, D. I., Swierczynski, M., Stan, A. I., Knap, V., Teodorescu, R., & Andreasen, S. J. (2014, September). Diagnosis of lithium-ion batteries state-of-health based on electrochemical impedance spectroscopy technique. In 2014 IEEE Energy Conversion Congress and Exposition (ECCE) (pp. 4576-4582). IEEE

[33] Galeotti, M., Cinà, L., Giammanco, C., Cordiner, S., & Di Carlo, A. (2015). Performance analysis and SOH (state of health) evaluation of lithium polymer batteries through electrochemical impedance spectroscopy. Energy, 89, 678-686.

[34] Lyu, C., Zhang, T., Luo, W., Wei, G., Ma, B., & Wang, L. (2019, June). SOH Estimation of Lithium-ion Batteries Based on Fast Time Domain Impedance Spectroscopy. In 2019 14th IEEE Conference on Industrial Electronics and Applications (ICIEA) (pp. 2142-2147). IEEE.

[35] De Sutter, L., Firouz, Y., De Hoog, J., Omar, N., & Van Mierlo, J. (2019). Battery aging assessment and parametric study of lithium-ion batteries by means of a fractional differential model. Electrochimica Acta, 305, 24-36.

[36] Olofsson, Y., Groot, J., Katrašnik, T., & Tavčar, G. (2014, December). Impedance spectroscopy characterisation of automotive NMC/graphite Li-ion cells aged with realistic PHEV load profile. In 2014 IEEE International Electric Vehicle Conference (IEVC) (pp. 1-6). IEEE.

[37] Wang, X., Wei, X., & Dai, H. (2019). Estimation of state of health of lithium-ion batteries based on charge transfer resistance considering different temperature and state of charge. Journal of Energy Storage, 21, 618-631.

[38] Xiong, R., Tian, J., Mu, H., & Wang, C. (2017). A systematic model-based degradation behavior recognition and health monitoring method for lithium-ion batteries. Applied Energy, 207, 372-383.

This document is the pre-print version of the article:
Locorotondo, E., Cultrera, V., Pugi, L., Berzi, L., Pierini, M., Lutzemberger, G., 2021. Development of a battery real-time state of health diagnosis based on fast impedance measurements. Journal of Energy Storage 38, 102566.
https://doi.org/10.1016/j.est.2021.102566

[39] Eddahech, A., Briat, O., & Vinassa, J. M. (2015). Performance comparison of four lithium–ion battery technologies under calendar aging. Energy, 84, 542-550.

[40] Love, C. T., Virji, M. B., Rocheleau, R. E., & Swider-Lyons, K. E. (2014). State-of-health monitoring of 18650 4S packs with a single-point impedance diagnostic. Journal of Power Sources, 266, 512-519..

[41] Christophersen, J. P., Morrison, J., Morrison, W., & Motloch, C. (2012). Rapid impedance spectrum measurements for state-of-health assessment of energy storage devices. SAE International Journal of Passenger Cars-Electronic and Electrical Systems, 5(2012-01-0657), 246-256.

[42] Haußmann, P., & Melbert, J. (2017). Optimized mixed-domain signal synthesis for broadband impedance spectroscopy measurements on lithium ion cells for automotive applications. Journal of Sensors and Sensor Systems, 6(1), 65.

[43] Relan, R., Firouz, Y., Timmermans, J. M., & Schoukens, J. (2016). Data-driven nonlinear identification of Li-ion battery based on a frequency domain nonparametric analysis. IEEE Transactions on Control Systems Technology, 25(5), 1825-1832.

[44] Sihvo, J., Stroe, D. I., Messo, T., & Roinila, T. (2019). Fast Approach for Battery Impedance Identification Using Pseudo-Random Sequence Signals. IEEE Transactions on Power Electronics, 35(3), 2548-2557.

[45] Locorotondo, E., Scavuzzo, S., Pugi, L., Ferraris, A., Berzi, L., Airale, A., ... & Carello, M. (2019, June). Electrochemical Impedance Spectroscopy of Li-Ion battery on-board the Electric Vehicles based on Fast nonparametric identification method. In 2019 IEEE International Conference on Environment and Electrical Engineering and 2019 IEEE Industrial and Commercial Power Systems Europe (EEEIC/I&CPS Europe) (pp. 1-6). IEEE.

[46] Al Nazer, R., Cattin, V., Granjon, P., Montaru, M., & Ranieri, M. (2013). Broadband identification of battery electrical impedance for HEVs. IEEE transactions on vehicular technology, 62(7), 2896-2905.

[47] Piret, H., Granjon, P., Guillet, N., & Cattin, V. (2016). Tracking of electrochemical impedance of batteries. Journal of Power Sources, 312, 60-69.

This document is the pre-print version of the article:
Locorotondo, E., Cultrera, V., Pugi, L., Berzi, L., Pierini, M., Lutzemberger, G., 2021. Development of a battery real-time state of health diagnosis based on fast impedance measurements. Journal of Energy Storage 38, 102566.
https://doi.org/10.1016/j.est.2021.102566

[48] Howey, D. A., Mitcheson, P. D., Yufit, V., Offer, G. J., & Brandon, N. P. (2013). Online measurement of battery impedance using motor controller excitation. IEEE transactions on vehicular technology, 63(6), 2557-2566.

[49] Serni, T., Locorotondo, E., Pugi, L., Berzi, L., Pierini, M., & Cultrera, V. (2020, June). A Low Cost Programmable Hardware for Online Spectroscopy of Lithium Batteries. In 2020 IEEE 20th Mediterranean Electrotechnical Conference (MELECON) (pp. 57-62). IEEE.

[50] Boukamp, B. A. (1995). A linear Kronig-Kramers transform test for immittance data validation. Journal of the electrochemical society, 142(6), 1885-1894.

[51] Schönleber, M., Klotz, D., & Ivers-Tiffée, E. (2014). A method for improving the robustness of linear Kramers-Kronig validity tests. Electrochimica Acta, 131, 20-27.

[52] L. Ljung, ”System Identification - Theory for the User”, Prentice Hall, 1999.

[53] Pintelon, R., & Schoukens, J. (2012). System identification: a frequency domain approach. John Wiley & Sons.

[54] J. Silva and N. Maia, ”Modal Analysis and Testing”, Applied Science, Vol. 363, 1999.

[55] Davies, W. D. T. (1970). System identification for self-adaptive control. Wiley Interscience, New York.

[56] Welch, P. (1967). The use of fast Fourier transform for the estimation of power spectra: a method based on time averaging over short, modified periodograms. IEEE Transactions on audio and electroacoustics, 15(2), 70-73.

[57] Al Nazer, R., Cattin, V., Granjon, P., Montaru, M., Ranieri, M., & Heiries, V. (2013). Classical EIS and square pattern signals comparison based on a well-known reference impedance. World Electric Vehicle Journal, 6(3), 800-806.

[58] EIG battery official site, www.eigbattery.com

[59] Andrenacci, N., & Sglavo, V. (2017). Stato dell'arte dei modelli di invecchiamento per le celle litio-ione. Applicazione al caso di studio delle celle NMC invecchiate in ENEA. Report RDS/PAR2016/163.